

# High frequency acoustic transmission loss of perforated plates at normal incidence

Vincent Phong<sup>a)</sup> and Dimitri Papamoschou

*Department of Mechanical and Aerospace Engineering, University of California, Irvine, California, 92697*

(Received 8 October 2012; revised 16 May 2013; accepted 30 May 2013)

A study has been conducted on the transmission loss of perforated plates at normal incidence. The investigation includes a theoretical analysis of the problem with validation through experimentation. The experiments comprised microphone measurements of transmission loss for 11 perforated plates with variable thickness, hole size, and porosity. The theoretical model is based on planar wave propagation through a single contraction/expansion chamber with modifications to account for hole interaction effects. The resulting formula for transmission loss yields superior predictions over past theories for the range of properties investigated. Deviations between experimental measurements and theoretical predictions of transmission loss are less than about 1.5 dB for dimensionless hole diameter  $d/\lambda < 0.5$ . The accuracy of the model does not show a strong dependence on plate thickness-to-diameter ratio or porosity.

© 2013 Acoustical Society of America. [<http://dx.doi.org/10.1121/1.4812271>]

PACS number(s): 43.58.Bh, 43.55.Ev, 43.20.Rz [FCS]

Pages: 1090–1101

## I. INTRODUCTION

Perforated material has been extensively employed in various noise control applications. Examples include acoustic liners for ducts and aeroengine nacelles, automotive mufflers, and silencers for flow control valves. Aeroengine acoustic liners and automotive muffler are classified as reactive silencers.<sup>1</sup> In reactive silencers, the frequency response of the system is tuned to suppress sound at targeted frequencies such as, for example, the blade passing frequency of a rotor or the firing frequency of an internal combustion engine. In these applications, the propagation of the predominant acoustic waves is typically at a grazing incidence to the perforations. In addition, grazing flow may be present.

Perforated plates are also used in mufflers for flow control valves, particularly pneumatic bleed valves on gas turbines.<sup>2</sup> These valves discharge compressor air into the fan duct of a turbofan engine to prevent compressor surges during transients or throttle back. Noise from the bleed valves can be a significant contributor to total aircraft noise. Figure 1 depicts a simplified drawing of a pneumatic bleed valve. It consists of a valve body, followed by a muffler comprising perforated plates oriented substantially normally to the mean flow direction. Typically two or more perforated plates are used. Without the muffler, the exhaust of the valve forms a high-speed turbulent jet that is very loud. The muffler expands the cross-sectional area of the flow and dramatically reduces its bulk velocity. The small jets emerging from the perforations produce noise at very high frequency, but this noise is attenuated rapidly by atmospheric absorption. What remains, though, is transmission of sound from the internal sources, including turbulence and vortex shedding through the perforations. Recent efforts to suppress bleed valve noise underscored the lack of fundamental

understanding of the dependence of sound attenuation on the properties of the perforated plate (porosity, hole size, thickness). This formed the basic motivation for the current study, namely the understanding and modeling of sound transmission through the perforated plates exemplified in Fig. 1. It is evident that the noise suppression mechanism does not involve tuning and is thus fundamentally different from reactive mufflers. However, the basic physics of sound transmission through a perforation remains relevant to both reactive and non-reactive applications.

It is important to outline the boundaries of the present investigation with further details to be presented in Sec. II. For the typical hole dimensions and operating frequencies of the bleed-valve muffler, the transmission process is dominated by inertial effects. Although a range of incidence angles is present in the actual application, it is fair to assume that the predominant incidence angle is normal. Therefore the current study is restricted to normal incidence angles. Non-linear effects on sound propagation through the orifice are deemed insignificant both for the actual device and the experiment of this study. Finally, the flow through the perforations can significantly affect the transmission loss. Here we assume that the orifice Mach number is small enough that the mean flow has negligible effects on the propagation.

The model problem of this study, therefore, is the inviscid, linear transmission of sound at normal incidence through a perforated plate. This is considered as a first step toward the modeling of the complex system illustrated in Fig. 1. Even though the research was motivated by bleed valve problems, its results will be generic enough for other applications as well. A notable feature of the experimental component of the study is the use of a broadband “point source” for the incident field; this enables the measurement of transmission loss over a wide frequency range in a single experiment. In addition, the measurement setup, to be discussed in Sec. III, avoids the limitations of impedance tubes with

<sup>a)</sup>Author to whom correspondence should be addressed. Electronic mail: [vphong@uci.edu](mailto:vphong@uci.edu)

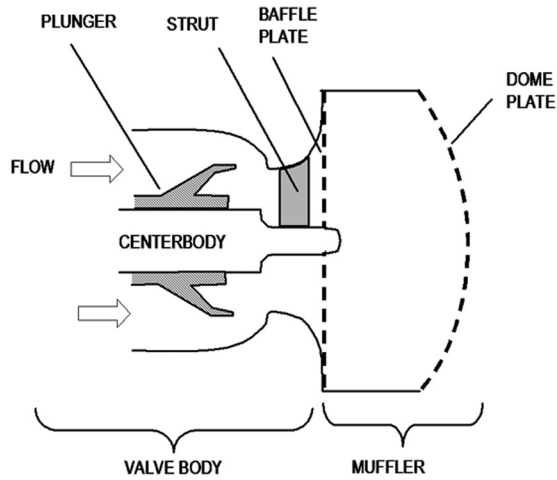


FIG. 1. Schematic of pneumatic bleed valve assembly used on aircraft engines (Ref. 2).

regard to the size of the sample to be tested. A large variety of perforated plates is considered to develop a comprehensive model of sound attenuation, validated by experimental measurements.

The structure of the paper is as follows: Sec. II reviews the fundamental physics of sound transmission through perforates, discusses past models that are relevant to this study, and proposes a new theoretical model for the transmission loss. Section III covers the experimental setup, and Sec. IV presents the experimental results on transmission loss with comparisons to the present model and appropriate past models. The paper concludes with Sec. V.

## II. THEORETICAL MODELING

In this section, we review fundamental principles pertinent to the current investigation, discuss past relevant theoretical works, and introduce a simple model for transmission loss the predictions of which will be compared to experimental measurements.

### A. Fundamental principles

Our investigation focuses on the transmission loss of perforated plates, namely the fraction of acoustic power that is transmitted through the plate. This is a process that is generally governed by inertial and viscous effects. As shown by Crandall,<sup>3</sup> the discriminant between viscous and inertial effects on sound propagation through a short tube is the quantity

$$\eta = \frac{1}{2} d \sqrt{\frac{\rho \omega}{\mu}}, \quad (1)$$

where  $d$  is the tube diameter,  $\omega$  is the angular frequency, and  $\rho$  and  $\mu$  are the density and dynamic viscosity of the fluid, respectively. For  $\eta \leq 1$ , the propagation is dominated by viscous effects. For  $\eta > 1$ , inertial effects become prominent. The discriminant can be rewritten using the acoustic propagation speed,  $c$ , and wavelength,  $\lambda$ , as

$$\eta = \sqrt{\frac{\pi \rho c d}{2 \mu}} \sqrt{\frac{d}{\lambda}}. \quad (2)$$

The argument of the first square root has the form of a Reynolds number based on the speed of sound and the hole diameter. The argument of the second square root is the non-dimensional hole size, an important parameter in the analysis that follows. For a hole diameter of 1 mm (the order of magnitude in this study), and for air at standard conditions, the discriminant becomes  $\eta = 184 (d/\lambda)^{1/2}$ . This means that inertial effects dominate down to  $d/\lambda \sim 10^{-4}$ , i.e., frequencies on the order of 30 Hz. Aerospace applications are typically concerned with much higher frequencies associated with peak levels of annoyance. We conclude that for the applications that motivated this study, the sound transmission process can be treated as purely inertial with a good degree of accuracy.

The sound field around the perforation consists of the incident, reflected, and transmitted waves (subscripts  $i$ ,  $r$ , and  $t$ , respectively). The acoustic power of each wave is  $\Pi = \overline{p' u'}$ , where  $p'$  is the pressure fluctuation,  $u'$  is the particle velocity, and  $\overline{(\ )}$  denotes time averaging. The transmission loss is defined as<sup>4</sup>

$$L_T = 10 \log_{10} \left[ \frac{\Pi_i}{\Pi_t} \right]. \quad (3)$$

Concerning the propagation of sound in a tube or lattice of tubes, we gain insight into the transmission loss by linking the acoustic power to the acoustic impedance. The acoustic impedance of a fluid acting over a surface area  $S$  is defined as the ratio of the acoustic pressure to the particle velocity

$$Z = \frac{1}{S} \frac{p'}{u'}. \quad (4)$$

Expressing the particle velocity in terms of the impedance and pressure fluctuation according to Eq. (4), the acoustic power follows the qualitative relation

$$\Pi \sim \frac{\overline{p'^2}}{|Z|}. \quad (5)$$

From Eq. (5), it is apparent that the power of the acoustic disturbance is maximized when the acoustic impedance is minimized. This occurs for disturbances at the resonance frequency of the system. Concerning the perforated plate, the incident wavefront acts as a source that disturbs the column of air inside the perforations. When the air is disturbed at integer multiples of its resonance frequency, the power of the acoustic waves inside the perforation is maximized. This results in maximum transmission of the energy from the incident wavefront through the perforations, or minimum transmission loss, at these characteristic frequencies.

Acoustic disturbances that propagate within the perforations disturb the medium adjacent to the ends of the perforation. This is illustrated in Fig. 2, where the dotted line represents the distribution of the disturbed, “attached” mass of a single hole. The disturbance inside the perforation travels a distance slightly further than the geometric thickness of

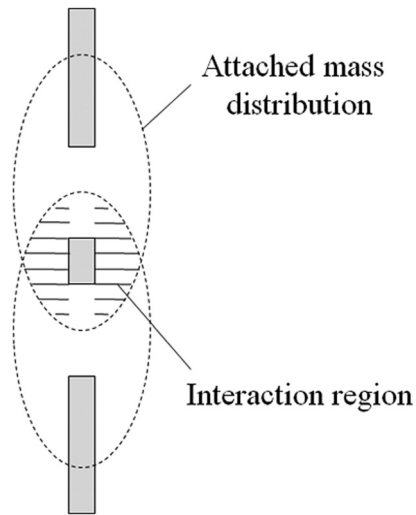


FIG. 2. Cutaway view of two holes, showing the attached mass distribution associated with each hole and the interaction region between both holes (Ref. 20).

the perforation as a result of this attached mass. This gives rise to an end correction to the perforation thickness, which was treated analytically by Rayleigh.<sup>5</sup> In the case of multiple adjacent holes, the attached mass regions overlap forming an interaction region whose extent is determined by the spacing between the holes (Fig. 2). The consequence of this interaction has been addressed by many authors. Fok<sup>6</sup> described the hole interaction effect (HIE) as a correction to Rayleigh's analysis on the acoustic conductivity of a single orifice. An analytical expression known as Fok's function was developed using potential theory (to be introduced in Sec. II C) and can be expressed in terms of the plate porosity  $\beta$ . Nesterov<sup>7</sup> validated Fok's work experimentally, showing that an increase in the porosity corresponds to a reduction in the end correction for thickness. Other investigators attributed HIE to the diffraction of pressure waves that radiate from the perforations. Ingard<sup>8</sup> showed that the pressure radiated from an orifice exerts an additional force on nearby orifices and that this effect is strongly dependent on the separation distance between perforations. He described this acoustic interaction by a correction term, the interaction impedance, to the acoustic impedance of an isolated orifice. Christensen<sup>9</sup> and Hou *et al.*<sup>10,11</sup> concluded that the diffracted waves created acoustic modes that travel parallel to the surface of the perforated plate. The interaction between the surface modes and diffracted pressure waves from the perforations modifies the resonance condition associated with the original plate thickness to a plate that is 16% thinner.<sup>10,11</sup> The aforementioned works<sup>6–11</sup> indicated that HIE results in scaling the end correction associated with a single orifice. In the current investigation, the HIE is accounted for using Fok's function with more details on this implementation in Sec. II C.

The transmission characteristics of an orifice exhibits nonlinear behavior at high pressure amplitudes because of the dissipative effects of the jet and vortex rings formed downstream of the orifice.<sup>12–14</sup> Ingard and Ising<sup>14</sup> observed a linear relationship between the acoustic pressure and particle

velocity for sound pressure levels (SPL) up to about 120 dB, with a quadratic relation starting above 130 dB. The SPL in the muffler cavity of Fig. 1 is estimated not to exceed 120 dB based on far-field measurements of the jet issuing from the isolated valve body. Acoustic levels in the experiment of this study are much lower, around 60 dB. For this reason, we conclude that non-linear effects are not significant in the actual application or the model experiment.

The effect of mean flow on the impedance of a single orifice or a perforated sheet has been addressed by a number of studies.<sup>15–17</sup> Experiments by Lee *et al.*<sup>16</sup> showed that the mean flow increases the impedance due to the dissipative effects of the jet developed downstream of the orifice. Aygun and Attenborough<sup>15</sup> demonstrated experimentally that the increase in transmission loss due to bias flow is strongly dependent on porosity. A transmission loss model for poroelastic plates with no bias flow was also presented in their work.

## B. Previous models

Models of past works that are relevant to the scope of the current investigation will now be reviewed. Chen<sup>18</sup> proposed a theoretical model, with experimental validation, for the transmission loss of a perforated plate under the assumption of a two-dimensional planar wave incident on a rigid screen. The screen dimensions were assumed to be large in comparison to the wavelength. The air column inside the perforation was assumed to move in phase, behaving like a rigid piston. Viscous losses were neglected. Transmission loss predictions were provided for  $0.002 < d/\lambda < 0.093$ ,  $0.0003 < l/\lambda < 0.0023$ , and were shown to agree well with the experiments. Chen accounted for the directivity of transmission loss by averaging over a hemisphere upstream from the perforated screen, resulting in the expression

$$L_T = -10 \log \int_0^{\pi/2} \left| \left[ i \frac{(l + \varepsilon)\omega}{2\beta c} \cos \theta + 1 \right]^{-2} \right| \sin 2\theta d\theta. \quad (6)$$

$\theta$  is the angle with respect to the normal direction of the plate surface,  $c$  is the propagation speed of the acoustic wave, and  $\beta$  is the porosity of the plate. The plate thickness  $l$  is augmented by an end correction factor  $\varepsilon$ , which was determined empirically to equal 1.6 times the perforation radius if the ratio of perforation radius to the distance between the holes was less than 0.2. For perforations with uniformly spaced holes, this translates to a porosity of 0.126 or less.

Tayong *et al.*<sup>19</sup> and Melling<sup>20</sup> defined the normal surface impedance of the perforations while incorporating Fok's function to account for HIE. Using the lumped acoustic impedance model formulated by Ingard,<sup>8</sup> Tayong *et al.* accounted for HIE in the reactance (imaginary) term of the impedance, resulting in the expression

$$Z_p = Z_{cav} + \frac{\sqrt{8\omega\rho\mu}}{\beta} \left( 1 + \frac{l}{d} \right) + \frac{i\omega\rho}{\beta} \left( l + \frac{8d}{3\pi\psi(\beta)} \right), \quad (7)$$

where  $Z_{\text{cav}}$  is the cavity impedance and  $\psi$  is Fok's function.  $Z_{\text{cav}}$  can be defined for a perforated panel surrounded on both sides by semi-infinite fluid media by defining  $Z_{\text{cav}}$  as the characteristic impedance of the fluid. This imposes the condition that there can be no reflected waves in the fluid media where the transmitted waves propagate. Tayong *et al.* also include additional terms to account for nonlinear effects in their work due to high sound pressure level excitations.<sup>15</sup> Because the scope of the current study is concerned only with the linear regime, these terms were neglected, resulting in Eq. (7). Experimental validation for their perforation impedance model is provided for  $0.0014 \leq d/\lambda \leq 0.0024$  and  $0.001 < l/\lambda < 0.002$ . Tayong *et al.* defined the reflection coefficient,  $R_c$ , as

$$R_c = \frac{Z_p - Z_0}{Z_p + Z_0}, \quad (8)$$

where  $Z_0 = \rho c$  is the characteristic impedance of air. To compare directly with the experimental measurements in this study, the transmission loss expression, Eq. (3), is rewritten using the transmission coefficient  $T_c = 1 - |R_c|^2$

$$L_T = -10 \log_{10}(T_c). \quad (9)$$

Substituting Eq. (8) into Eq. (9) results in an expression for transmission loss as a function of the perforation impedance

$$L_T = -10 \log_{10} \left( 1 - \left| \frac{Z_p - Z_0}{Z_p + Z_0} \right|^2 \right). \quad (10)$$

An alternative modeling approach treats the perforations as an effective fluid layer.<sup>11,21–24</sup> The perforated plate is assumed to be rigid and porous with circular cylindrical pores. The effective density,  $\rho_e$ , and bulk modulus,  $K$ , can be defined using the Johnson—Champoux—Allard model<sup>23</sup>

$$\rho_e = \rho \alpha_\infty \left[ 1 + \frac{\sigma \beta}{i \omega \rho \alpha_\infty} \left( 1 + i \frac{\rho \omega \alpha_\infty}{2 \sigma \beta} \right)^{1/2} \right], \quad (11)$$

$$K = \frac{\gamma p_0}{\gamma - (\gamma - 1) \left[ 1 + \frac{\sigma \beta}{i \text{Pr} \omega \rho \alpha_\infty} \left( 1 + i \frac{\rho \text{Pr} \omega \alpha_\infty}{2 \sigma \beta} \right)^{1/2} \right]^{-1}}, \quad (12)$$

where the flow resistivity is  $\sigma = 32\mu/\beta d^2$ , the geometric tortuosity is  $\alpha_\infty = 1$ , and  $\gamma$ ,  $p_0$ ,  $\rho$ , and  $\text{Pr}$  are the specific heat ratio, static pressure, density, and Prandtl number for air, respectively, at 18 °C ( $\gamma = 1.4$ ,  $p_0 = 1.013 \cdot 10^5$  Pa,  $\rho = 1.21$  kg/m<sup>3</sup>, and  $\text{Pr} = 0.71$ ). Atalla and Sgard<sup>21</sup> proposed a correction to the geometric tortuosity by accounting for flow distortions within the vicinity of the perforations

$$\alpha_\infty = 1 + 2 \frac{\varepsilon}{l}, \quad (13)$$

where  $\varepsilon$  is an end correction length defined by Jaouen and Bécot<sup>24</sup> as  $\varepsilon = (1 - 1.13\xi - 0.09\xi^2 + 0.27\xi^3)8r/3\pi$  with  $\xi = 2\sqrt{\beta/\pi}$ . The effective characteristic impedance and

wavenumber of the perforated plate is defined using Eqs. (11)–(13)

$$Z_{0,p} = \sqrt{K \rho_e}, \quad (14)$$

$$k_p = \omega \sqrt{\frac{K}{\rho_e}}. \quad (15)$$

Assuming that the semi-infinite fluid media on both sides of the perforation is air, the Transfer Matrix Method<sup>25</sup> (TMM) can be applied, using Eqs. (14) and (15), to determine the transmission loss

$$L_T = 20 \log_{10} \left\{ \left| \cos(k_p l) + \frac{i}{2} \left[ \frac{Z_{0,p}}{\beta Z_0} + \frac{\beta Z_0}{Z_{0,p}} \right] \sin(k_p l) \right| \right\}, \quad (16)$$

where  $Z_0$  is the characteristic impedance of air. Atalla and Sgard provided experimental validation for their perforation impedance model for  $3 \times 10^{-5} \leq d/\lambda \leq 0.0295$  and  $3 \times 10^{-5} < l/\lambda < 0.015$ .

### C. Present theoretical formulation

In the present study, the transmission loss of the perforate is modeled theoretically by considering a duct containing a single contraction chamber, as illustrated in Fig. 3. The development follows the inertial model of Ffowcs Williams and Dowling<sup>26</sup> with important modifications related to end effects.

Besides the neglect of viscous effects, the other major assumption is that the wavelength of sound is larger than the contraction diameter, which allows the approximation of the sound waves throughout the duct as one dimensional.<sup>26</sup> Acoustic waves that are confined spatially to regions such as ducts will have modes that will propagate or decay, depending on the frequency of excitation.<sup>25</sup> If the waves in the duct are excited at a frequency below the cutoff frequency of a certain mode, the mode is considered evanescent and will decay at appreciable distances from the source. The plane wave assumption restricts the model accuracy to only frequencies below the cutoff frequency corresponding to plane wave propagation inside perforations. If the perforations are approximated as circular ducts, the cutoff frequency can be expressed non-dimensionally as  $d/\lambda = 0.5861$ .

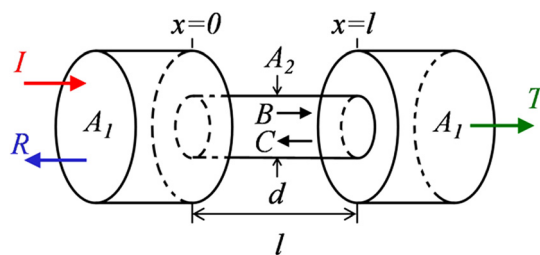


FIG. 3. (Color online) Contraction chamber used for 1D modeling of transmission (Ref. 26).

The acoustic pressures throughout the domain are expressed as

$$\begin{aligned} p' &= I e^{i\omega(t-x/c_1)} + R e^{i\omega(t+x/c_1)}, & x < 0 \\ p' &= B e^{i\omega(t-x/c_2)} + C e^{i\omega(t+x/c_2)}, & 0 \leq x \leq l \\ p' &= T e^{i\omega(t-x/c_3)}, & x > l \end{aligned} \quad (17)$$

where  $I$ ,  $R$ , and  $T$  are the amplitudes of the incident, reflected, and transmitted waves, respectively. The subscripts 1, 2, and 3 will be used as reference to the regions upstream, inside, and downstream of the contraction, respectively. The amplitudes  $B$  and  $C$  of the pressure waves inside the contraction are determined by application of the conservation equations. The mass flux into the contraction interface ( $x=0$ ) must equal the mass flux out of the contraction.

$$\rho A_1 u'_1 = \rho A_2 u'_2. \quad (18)$$

In addition, the energy flux into the contraction interface must equal the energy flux out of the contraction.

$$A_1 p'_1 u'_1 = A_2 p'_2 u'_2. \quad (19)$$

Combining Eqs. (18) and (19) shows that the energy flux condition is a statement of continuity in the acoustic pressure at the contraction interface,  $p'_1 = p'_2$ . The same conditions of mass and energy flux apply at the expansion interface ( $x=l$ ). Assuming that the pressure fluctuations propagate at the same speed throughout the entire domain ( $c=c_1=c_2=c_3$ ), these conditions yield the following set of algebraic equations that relate  $R$  and  $T$  to  $I$ :

$$T = \frac{2I e^{i\omega l/c}}{2 \cos\left(\frac{\omega l}{c}\right) + i \left[ \frac{A_1}{A_2} + \frac{A_2}{A_1} \right] \sin\left(\frac{\omega l}{c}\right)}, \quad (20)$$

$$R = \frac{iI \left[ \frac{A_1}{A_2} - \frac{A_2}{A_1} \right] \sin\left(\frac{\omega l}{c}\right)}{2 \cos\left(\frac{\omega l}{c}\right) + i \left[ \frac{A_1}{A_2} + \frac{A_2}{A_1} \right] \sin\left(\frac{\omega l}{c}\right)}. \quad (21)$$

It can be shown from Eqs. (20) and (21) that the sum of the energies in the reflected and transmitted waves equals the energy of the incident wave

$$|R|^2 + |T|^2 = |I|^2. \quad (22)$$

In other words, this is a lossless process as evident from the lack of any dissipative (viscous) effects in the formulation of the governing equations. Adopting Eq. (3) to the current problem, the transmission loss is

$$L_T = 10 \log_{10} \left( \frac{|I|^2}{|T|^2} \right). \quad (23)$$

Substituting Eq. (20)

$$L_T = 10 \log_{10} \left[ 1 + \frac{1}{4} \left( \frac{A_1}{A_2} - \frac{A_2}{A_1} \right)^2 \sin^2 \left( \frac{\omega l}{c} \right) \right]. \quad (24)$$

In applying Eq. (24) to a perforated plate, the porosity is  $\beta = A_2/A_1$ , and the plate thickness is  $l$ . It is noted that the transmission loss in Eq. (24) is symmetric in  $A_1$  and  $A_2$  and is thus the same whether the chamber is expanding ( $A_2 > A_1$ ) or contracting ( $A_2 < A_1$ ). With these substitutions, Eq. (24) becomes

$$L_T = 10 \log_{10} \left[ 1 + \frac{1}{4} \left( \frac{1}{\beta} - \beta \right)^2 \sin^2(kl) \right] \quad (25)$$

with  $k = \omega/c$  being the acoustic wavenumber.

As discussed in Sec. II A, an end correction for the thickness must be applied to account for the effect of acoustic interaction between the holes of the perforated plate.<sup>6-11</sup> The thickness of the plate is replaced with an effective thickness

$$l_e = l + \varepsilon d, \quad (26)$$

where  $d$  is the hole diameter and  $\varepsilon$  is a correction factor defined as

$$\varepsilon = \frac{8}{3\pi\psi(\xi)}. \quad (27)$$

The  $8/(3\pi)$  term in Eq. (27) is the end correction applicable to a single orifice in a spatially infinite plate.<sup>5</sup> The additional term in the denominator,  $\psi(\xi)$ , originates from the work of Fok,<sup>6</sup> who considered the problem of a circular tube of diameter,  $D$ , with a partition containing a circular orifice of diameter,  $d$ , located on the axis of the tube. His analysis shows that as  $d/D$  approaches unity, the orifice conductivity becomes infinite, and the end correction tends to zero. Conversely, for  $d/D \ll 1$ , the end correction approaches the value for a single orifice in an infinite plate,  $8/(3\pi)$ . Fok derived a function that describes this behavior

$$\begin{aligned} M(\xi) &= 1 - 1.40925 \xi + 0.33818 \xi^3 + \dots \\ &= 0.06793 \xi^5 - 0.02287 \xi^6 + \dots \\ &= 0.03015 \xi^7 - 0.01641 \xi^8 \end{aligned} \quad (28)$$

where  $\psi(\xi) = [M(\xi)]^{-1}$  is the reciprocal of Fok's function and its argument  $\xi = d/D$ . Nesterov<sup>7</sup> showed experimentally that Eq. (28) is valid for both single and multiple orifices. The case of multiple orifices is representative of a perforated plate where each orifice is confined within a lattice of characteristic length  $D$ , and the ratio of orifice area to lattice area is equal to the porosity  $\beta$  of the perforated plate. Nesterov showed that the effect of lattice geometry on Fok's function is negligible, indicating that the end correction associated with the perforations are independent of the nature of perforation grating. From this result, a circular lattice geometry of diameter  $D$  can be assumed for all perforated plates, and ratio of perforation area to lattice area, or porosity, can be defined as  $\beta = d^2/D^2$ . The argument in Fok's function can therefore be rewritten, using porosity, as  $\xi = \sqrt{\beta}$ . As  $\beta$  approaches zero, the lattice area effectively becomes infinite with respect to the perforation and  $\psi(0) = 1$ , resulting in an

end correction equal to a single orifice [Eqs. (27) and (28)]. Fok's function modifies the effective thickness of a single orifice in an infinite baffle by accounting for finite lattice area. Nesterov's experiments show that HIE are negligible for  $\beta < 0.10$ . The porosities of the perforations used in the current work are greater than 0.22, indicating that interaction effects must be considered for all the perforations considered here (Table I).

Incorporating the effective thickness, Eq. (25) becomes

$$L_T = 10 \log_{10} \left\{ 1 + \frac{1}{4} \left( \frac{1}{\beta} - \beta \right)^2 \sin^2 \left[ k \left( l + \frac{8d}{3\pi\psi(\sqrt{\beta})} \right) \right] \right\}. \quad (29)$$

Equation (29) is a variant of the original result by Ffowcs Williams and Dowling,<sup>26</sup> modified to include end corrections and HIE. It is noted that the transmission loss model contains a sine-squared term and therefore will exhibit oscillatory behavior that is governed by the effective thickness. The oscillatory behavior is caused by standing-wave-formed resonances inside the contraction that are analogous to Fabry-Pérot resonance observed in optics.<sup>9-11</sup> The transmission loss predicted by Eq. (29) will be compared to experimental results of transmission loss and to the previous theoretical models noted in Sec. II B.

### III. EXPERIMENTAL SETUP

#### A. Perforations

Eleven perforated plates of varying porosity, hole size, and thickness were investigated. Table I lists the perforation properties. All the plates were made of sheet metal: Either brass or steel. It was noted in a previous study<sup>14</sup> that the transmission characteristics of the plate is independent of its material composition. The test matrix includes a solid perforated plate (experiment S) and the free-field, baseline case (experiment 0). The gratings of the perforations on the plates were either square or triangular patterned.

TABLE I. Properties of perforated sheets used in experiments.

Experiment	Porosity $\beta$	Thickness $l$ (mm)	Hole diameter $d$ (mm)	Hole spacing $a$ (mm)	Perforation Grating
S	0.00	0.6096	—	—	—
0	1.00	—	—	—	—
1	0.37	0.6096	1.1430	1.676	Square
2	0.48	0.4064	2.6162	3.353	Square
3	0.37	0.4064	1.1430	1.676	Square
4	0.29	0.4064	1.0160	1.676	Square
5	0.45	0.7620	1.7526	2.794	Triangular
6	0.23	0.7620	1.5875	3.175	Triangular
7	0.23	0.9144	1.5875	3.175	Triangular
8	0.23	0.4064	0.6858	1.270	Square
9	0.23	0.4064	0.6096	1.118	Square
10	0.22	0.4064	0.5080	1.016	Triangular
11	0.22	0.4064	0.4064	0.889	Triangular

#### B. Acoustic measurement

The experimental setup for measurement of transmission loss has some similarity to the arrangement used by Chen.<sup>18</sup> The basic layout is shown in Fig. 4. Acoustic measurements were conducted inside an anechoic facility using two 3.2-mm condenser microphones (Brüel and Kjaer, model 4138) with frequency response of 120 kHz. The microphones were mounted inside a separate small anechoic box located within the anechoic facility. The anechoic box, detailed in Fig. 4, had one open side on which the perforated sheets were mounted. The other sides were lined with anechoic wedges with cut-off frequency of 200 Hz. The microphones were held on an arm at the opposite end of the box and were separated from each other by a distance of 76 mm. The distance between the microphone tips and plane of the opening was approximately 76 mm. A localized broadband acoustic source ("point source") was generated using four small impinging jets, each issuing from a 2.54-mm diameter tube and supplied at a pressure of 200 kPa. The design of the impinging-jets source was similar to that used by Gerhold and Clark.<sup>27</sup> The distance between the impinging-jets source and the perforated plate was 1.480 m. The perforated sheets were attached to the open end of the box using spring clamps. The box was hinged in one corner to allow variation of the incidence angle relative to the wave

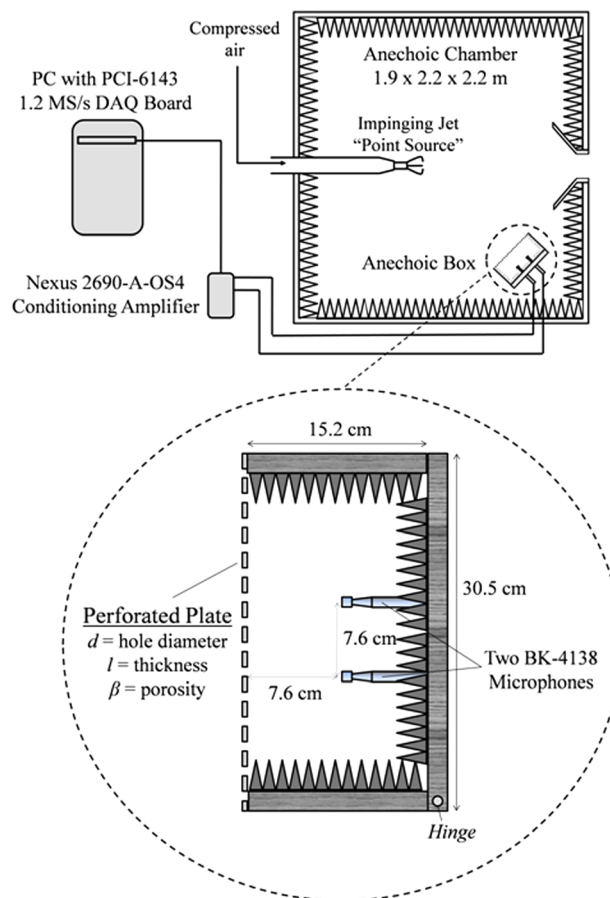


FIG. 4. (Color online) Schematic of experiment setup inside anechoic chamber, detailing the measurement setup in the anechoic box.

front. In the present experiments, the incidence angle was normal to the perforations.

Simultaneous data acquisition at a sampling rate of 250 kHz per channel was performed using two analog-to-digital boards (National Instruments PCI-6143) installed in a Dell Precision T7400 computer with a Xeon quad-core processor. The resulting signals were conditioned with a high-pass filter set at 300 Hz and a low-pass filter set at 140 kHz. Narrowband SPL spectra were computed using a 4096-point ( $\Delta f = 61$  Hz) fast Fourier transform and were corrected for microphone frequency response, free field response, and atmospheric absorption. The simultaneous acquisition enabled cross correlations between the two microphones. For the purpose of measuring the SPL relevant to transmission, the SPLs of the two microphones were averaged. To facilitate the interpretation of the transmission loss data, the spurious wiggles from the spectra were removed by using a Savitzky–Golay filter.<sup>28</sup> The filter removes the wiggles but does not alter the fundamental shape of the spectrum. Assuming plane-wave propagation, the transmission loss  $L_T$  of the perforated plate is defined as the difference in SPL between the open box (baseline case) and the box covered with the perforated plate.

#### IV. RESULTS

The results are presented in three sections. The first section evaluates the robustness of the experimental setup to accurately measure transmission loss. In the second section, the cross correlation of the two microphones was examined for ascertaining the plane-wave assumptions underpinning our model. The transmission loss results and comparisons to theoretical models are presented in the third section.

##### A. Robustness of setup

It was necessary to check for any possible sources of error in the experiment setup to ensure accuracy in the transmission loss measurements. Acoustic contamination could result from leaks due to inadequate sealing of the contact area between the perforated plate and the structure of the anechoic box. An additional source of concern is vibrations of the plate itself, which could lead to discrepancies in the transmission loss measurement. To assess these possible sources of error, experiments were conducted with a solid plate, and the results were compared to a perforated plate of equal thickness.

Figure 5 shows the raw SPL spectra (before smoothing) comparisons among three cases: The solid plate, the perforated plate, and the background noise with the source turned off and the solid plate installed. It is noted that the spectrum for the solid plate is well below the spectrum of the perforated plate. The difference is 20 dB at low frequency increasing to 50 dB at high frequency. This shows that the effects of vibration and leakage are very small and do not have any impact on the measured transmission loss. It is also noted that the spectrum for the solid plate is higher than the background spectrum, indicating some transmission of sound through the sealed anechoic box. It is natural that some sound will be transmitted through the box, particularly

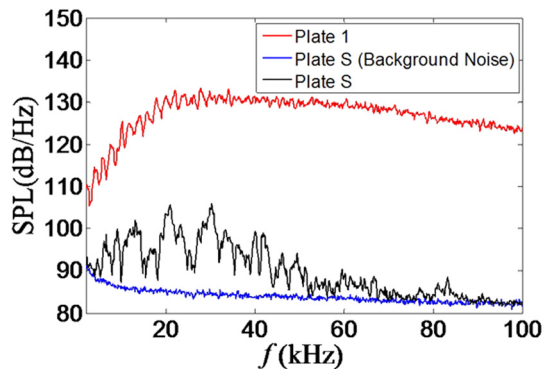


FIG. 5. (Color online) Comparisons of SPL spectra between perforated sheet and solid plate of equal thickness.

though the uninsulated solid plate. However, this transmission is extremely weak to influence the results.

##### B. Cross-correlations

To confirm that the incident waves were normal to the perforations, the signals of the two microphones were cross correlated. The microphone voltage signals were cross-correlated using MATLAB's inbuilt cross correlation function. Figure 6 plots the cross-correlation coefficient  $R_{m1m2}$  for the open box and the box covered with a perforated plate. For both the open and covered box, the cross-correlation peaks at  $\tau = 7.8 \mu\text{s}$ . This time lag corresponds to a propagation distance of 2.7 mm, which is very small compared to the 76-mm separation between the microphones. For all practical purposes, the sound arrives at the two microphones simultaneously, and the wavefronts are aligned with the plane of the perforation. It is interesting that the magnitude of the cross correlation does not decline with installation of the perforated plate. This indicates that the diffraction process is largely deterministic.

Further insight is gained by examining the coherence between the microphone signals, plotted in Fig. 7. The coherence  $\gamma^2$  was computed using MATLAB's inbuilt coherence function, using an FFT size of 4096 with a 1024 point Hanning window. The coherence plots are virtually identical for the open and covered box. The coherence is very strong for  $f < 100$  kHz, then falls off rapidly for higher frequency. The

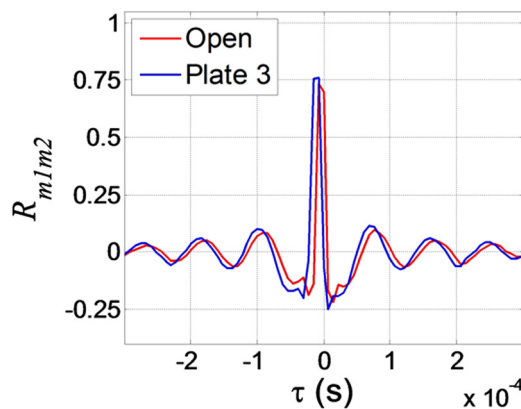


FIG. 6. (Color online) Cross correlation of microphone signals for the box without the perforated plate (open) and with perforated plate attached (plate 3).

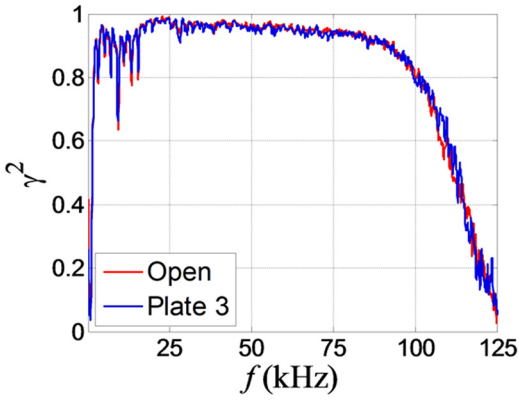


FIG. 7. (Color online) Coherence between microphone signals for the box without the perforated plate (open) and with perforated plate attached (plate 3).

decline has to do with the turbulent nature of the impinging-jets noise source wherein the variance of source location becomes large compared to the acoustic wavelength.

The cross-correlation results, in conjunction with the geometry of the setup depicted in Fig. 4, allow us to assess the applicability of the 1D propagation model, proposed in Sec. II C, to the present experiments. The strong coherence for  $f < 100$  kHz indicates a highly coherent wavefront impinging on the plate—a prerequisite for the aforementioned model. On the other hand, the decline in coherence for  $f > 100$  kHz indicates that the wavefronts impinging on individual holes become progressively uncorrelated. For this reason, only the results below 100 kHz are used in evaluating the model.

The large distance between the sound source and the perforated plate ensures that the wave approaching each hole is planar. Near the center of the plate, the incidence of the plane wave is normal. Toward the edge of the plate, the incidence is slightly off-normal with an obliquity angle no larger than  $6.4^\circ$ . Sustained propagation at such angle requires high-order radial and circumferential modes the cutoff frequency of which is much higher than the planar-propagation cutoff frequency mentioned in Sec. II C.<sup>29,30</sup> Therefore the obliquity of the incident wave on the perforations will not trigger any transverse modes and thus will not alter the transmission-loss relations developed in this paper.

### C. Transmission loss

The experimental results for transmission loss of the perforated plates listed in Table I are plotted in Fig. 8(a). For all the cases investigated, the transmission loss is practically zero at very low frequency. With increasing frequency, the transmission loss for plates with thickness  $l = 0.4046$  mm increases monotonically within the frequency range investigated. For the three cases with  $l > 0.4046$  mm (plates 5-7), the transmission loss curves rise then fall. As indicated in Sec. II C, the saturation and decline of transmission loss for the thick plates is a result of Fabry-Pérot-like resonance. The theoretical predictions for transmission loss are plotted in Fig. 8(b). A quick comparison between Figs. 8(a) and 8(b) shows that the model captures the experimental trends. In the cases with  $l > 0.4046$  mm, Eq. (29) is able to accurately predict the frequency at which the maximum transmission

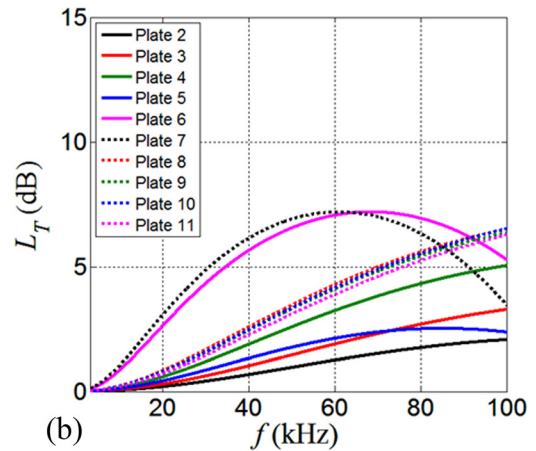
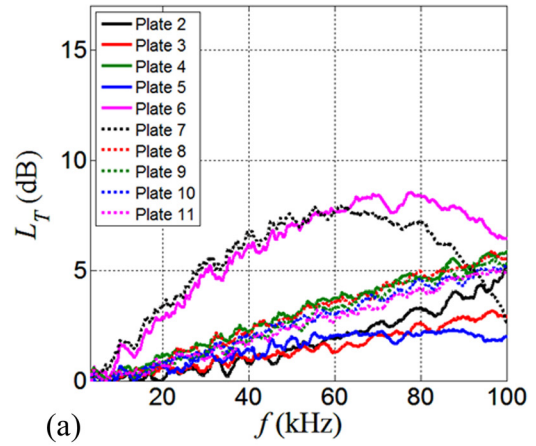


FIG. 8. (Color online) Transmission loss versus frequency. (a) Experiment; (b) proposed theoretical model Eq. (29).

loss occurs. The frequency limitation of the experiment prevented resolution of the frequency of peak transmission loss for plates with thickness  $l = 0.4046$  mm; therefore no distinct transmission loss maxima are observed for these cases. The comparisons in Fig. (8) also indicate a significant deviation between model and experiment at high frequency for plate 2. This deviation may be attributable to diffraction effects similar to Wood's anomaly,<sup>9-11,31</sup> which occurs when the wavelength becomes similar to the hole spacing. Plate 2 is the only case that may be impacted by Wood's anomaly within the experimental frequency range.

It is necessary to determine the range where the non-dimensional parameters of the previous classical models were validated so that comparisons with the current model can appropriately be made. The ratio of plate thickness to acoustic wavelength,  $l/\lambda$ , and perforation diameter to acoustic wavelength,  $d/\lambda$ , were selected as the relevant non-dimensional parameters. The range of  $d/\lambda$  and  $l/\lambda$  where the classical models were considered valid is determined based on their respective experimental constraints and is illustrated in Fig. 9. A region of significant overlap,  $0.002 < d/\lambda < 0.09$ , was chosen to compare the transmission loss results. It is shown in Fig. 9 that the current work investigates values of  $d/\lambda > 0.1$  and  $l/\lambda > 0.02$ , a region where previous classical models lack validation.

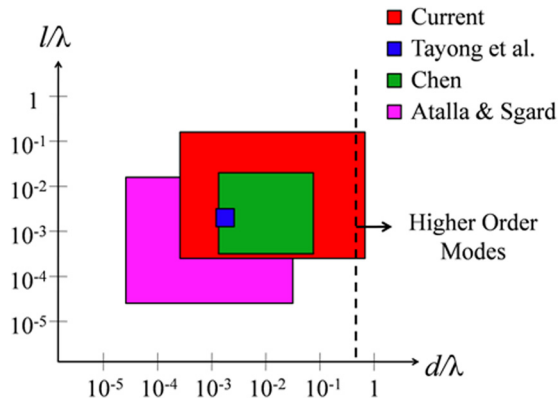


FIG. 9. (Color online) Comparisons of the range of  $d/\lambda$  and  $l/\lambda$  covered in the current and previous work. The ranges of  $d/\lambda$  and  $l/\lambda$  are determined based on the range of experimental validation provided for the respective work. The vertical dashed line indicates the cutoff  $d/\lambda$  above which nonplanar modes may propagate.

Figure 10 compares our transmission loss measurements with the predictions of the current model, Eq. (24), and the predictions by Chen,<sup>18</sup> Tayong *et al.*,<sup>19</sup> and Atalla and Sgard.<sup>21</sup> Equations (10) and (16) were used to recast the impedance expressions of Tayong *et al.* and Atalla and Sgard, respectively, into transmission loss. Figures 10(b), 10(f), and 10(g) focus on transmission loss between  $0.002 < d/\lambda < 0.09$ , the region of validity of the classical models. Figures 10(a), 10(c), 10(d), and 10(e) include results for  $d/\lambda > 0.09$ , and a vertical dashed line marking the upper  $d/\lambda$  limit at which classical models were validated.

Within the region of validated  $d/\lambda$ , Chen's theory overpredicts the transmission loss with increasing error at higher  $d/\lambda$  for all perforates. It is important to note that the end correction value used in Chen's theory is 0.8 times the

perforation diameter for  $\beta < 0.126$ . Because no specification was given for perforates with larger values of porosity, it is expected that Chen's theory will be inaccurate for higher porosity cases, such as plates 1, 2, and 5 [Figs. 10(a)–10(c)]. Both transmission loss predictions using the surface impedance model of Tayong *et al.* and applying the TMM to Atalla and Sgard's model agree well with the current experimental data within the region of validated  $d/\lambda$ , except for Plates 9 and 11 [Figs. 10(f) and 10(g)].

The capability of the classic and current models in predicting the resonance phenomena shown in the experiments [Fig. 8(a)] is compared next. Figures 10(a), 10(c), 10(d), and 10(e) indicate that resonance effects become apparent for  $d/\lambda > 0.1$ , a region that previous classical models<sup>18,19,21</sup> lack validation. This effect is an essential physical mechanism that cannot be ignored when modeling the transmission behavior of perforated plates. This underscores the distinguishing advantage of the current model over the model of Tayong *et al.* and Chen. As discussed in Sec. II B, the transmission loss was obtained from the model of Tayong *et al.*<sup>19</sup> by examining the classic problem of acoustic wave transmission between two semi-infinite fluid media: One defined by characteristic impedance of air and the other by the perforation impedance. Conservation equations are applied at the interface separating the media, resulting in the well known expression for reflection coefficient [Eq. (8)]. The transmission loss is then obtainable from the reflection coefficient, as shown in Eq. (10). In the current model, boundary conditions are applied at the two cross-sectional area changes of contraction chamber (Fig. 3). Reflected waves form within the contraction, resulting in a Fabry–Pérot-like resonance behavior when the acoustic wavelength approaches the order of the plate thickness  $l$ . This effect is captured in the transmission loss expression, Eq. (29), through the sine-squared

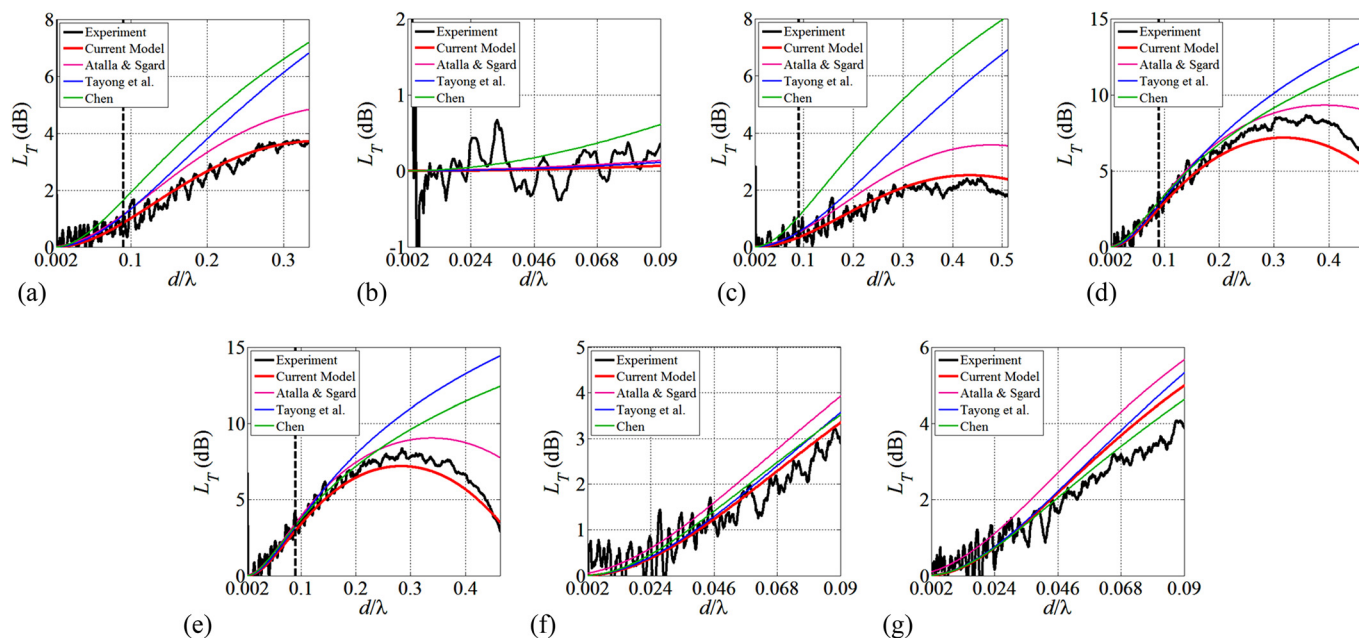


FIG. 10. (Color online) Comparison of transmission loss between experiment, proposed theoretical model Eq. (24), and previous models (Refs. 18, 19, and 21): (a) plate 1, (b) plate 2, (c) plate 5, (d) plate 6, (e) plate 7, (f) plate 9, (g) plate 11. The vertical dashed line indicates the upper limit of  $d/\lambda$  to which previous models were validated.

term, and is confirmed by experimental results for thicker plates.

The model of Atalla and Sgard<sup>21</sup> model was used in conjunction with the TMM to assess the accuracy to which their model can capture the resonance behavior shown in the current experiments. The results indicate that the Fabry–Pérot resonance behavior for thick plates is resolved with good accuracy in predicting the  $d/\lambda$  value of peak transmission loss. However, the model also yields large errors in transmission loss amplitude for plates 1, 5, and 7 [Figs. 10(a), 10(c), and 10(e)] at high  $d/\lambda$ . It is not expected, however, for the model of Atalla and Sgard to be accurate at high frequencies, or high  $d/\lambda$ , because their model was designed to focus on visco-inertial and thermal dissipative effects on the transmission behavior of porous media at low frequencies.

#### D. Accuracy of current prediction

To assess the range of validity of the current predictive model, Eq. (29), the deviation of the prediction from the experiment will be examined systematically. The error in transmission loss is defined as

$$\Delta L_T = L_{T,Model} - L_{T,Experiment}. \quad (30)$$

Equation (30) is plotted versus the relevant non-dimensional parameters of the problem. In the formulation of the current theory, it was assumed that the wavelength of sound is much greater than the perforation diameter. To examine the effect of this assumption, Fig. 11 plots  $\Delta L_T$  against the ratio of perforation diameter to wavelength of sound,  $d/\lambda$ , for all the plates examined. There is a very modest increase in  $\Delta L_T$  with increasing  $d/\lambda$ , the deviation being less than about 1.5 dB for  $d/\lambda < 0.5$ . For  $d/\lambda$  above this value,  $\Delta L_T$  increases significantly, as shown in the case of plate 2.

Because the current experiments include  $d/\lambda$  greater than the cutoff value of 0.5861 (Sec. II C), we expect the departure from the model, Eq. (30), to increase for  $d/\lambda > 0.5861$  because the acoustic excitations may contain nonplanar modes. This is evident in the trends of  $\Delta L_T$  in Fig. 11. For plate 2,  $\Delta L_T$  increases to about 2 dB at  $d/\lambda = 0.6$  and continues to increase monotonically with increasing  $d/\lambda$ .

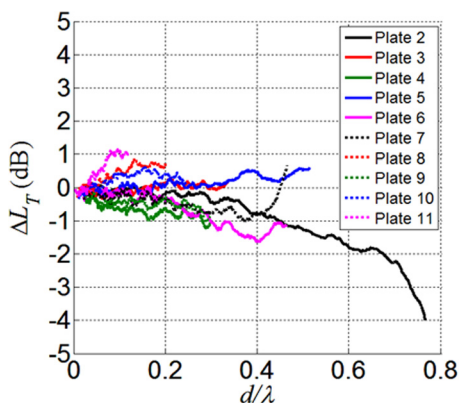


FIG. 11. (Color online) Transmission loss error versus perforation hole diameter scaled by acoustic wavelength.

It is concluded that the assumption of 1D propagation holds satisfactorily for  $d/\lambda < 0.5$ , where  $|\Delta L_T| \leq 1.5$  for all cases.

In addition to higher-order duct modes, it is expected that the diffracted pressure field will significantly influence the experimental results. The simplified analysis and assumptions made in formulating the problem do not allow a rigorous analysis of diffraction effects. It is believed, however, that diffraction effects are inherent in the application of end corrections. As discussed in Sec. II A, recent studies have attributed the effects of diffraction as a link between acoustic modes within the perforations and evanescent modes along the surface of the perforated plate.<sup>9–11</sup> It was shown in the works of these authors that the coupling between modes results in decreasing the Fabry–Pérot predicted resonance frequency. In the current model, the end correction with HIE increases the effective thickness of the plate, which also results in decreasing the resonance frequency. The similarity between these results implies a coupling between diffraction effects and the implementation of HIE using end corrections with Fok’s function. The validity of this assumption is corroborated by the accuracy in predicting the  $d/\lambda$  of peak transmission loss [Figs. 10(a), 10(c), 10(d), and 10(e)].

Next, the effects of dimensionless thickness and porosity on the model accuracy for  $d/\lambda < 0.5$  are examined. The effect of thickness-to-diameter ratio,  $l/d$ , on the transmission loss error is shown in Fig. 12 for several values of  $d/\lambda$ . The trends in Fig. 12 indicate that the transmission loss error is not a strong function of  $l/d$ . The magnitude of the error is less than 1.2 dB. Similarly, Fig. 13 plots  $\Delta L_T$  against the range of perforation porosities tested,  $0.22 < \beta \leq 0.48$ . The results of Fig. 13 show that the current model predicts the transmission loss within an error of about 1.2 dB or less for all the porosities tested. Unlike the trends seen in Fig. 11, where  $\Delta L_T$  increases with  $d/\lambda$ , there does not appear to be any definable trend between  $\Delta L_T$  and  $l/d$  or  $\beta$ .

Estrada *et al.*<sup>31</sup> and many other authors<sup>9–11</sup> indicated deviations from expected transmission behavior, known as Wood’s anomaly, when the acoustic wavelength approaches the same length as the spacing between perforations. This phenomenon occurs as a result of diffraction of higher order acoustic modes that cannot be resolved by the current

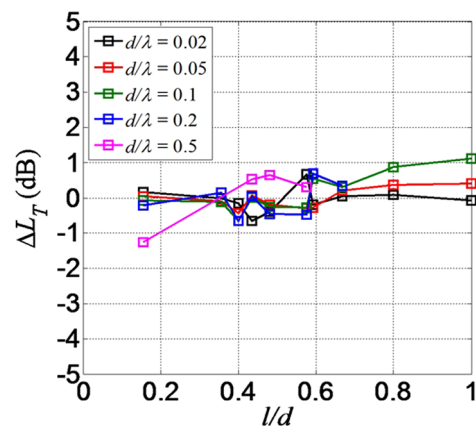


FIG. 12. (Color online) Transmission loss error versus non-dimensional plate thickness for varying  $d/\lambda$ .

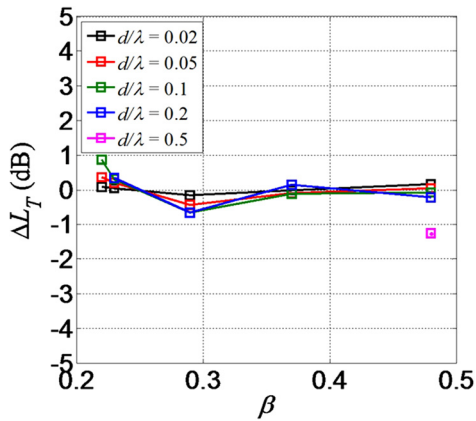


FIG. 13. (Color online) Transmission loss error versus perforate porosity for varying  $d/\lambda$ .

model's plane wave based approach. It is therefore expected that  $\Delta L_T$  will increase as  $\lambda$  approaches  $a$ . The spacing between the perforations in plate 2 approach this limit, which may possibly explain the large departure of experiment from the model prediction shown in Fig. (8).

## V. CONCLUSIONS

An experimental and theoretical parametric investigation of the acoustic transmission of perforated plates at normal incidence was conducted. The experiments utilized a broadband point source to evaluate the transmission loss of 11 perforated plates with varying porosity, hole size, and thickness. The experimental matrix covered porosities  $0.22 \leq \beta \leq 0.48$ , non-dimensional hole size  $7 \times 10^{-5} \leq d/l \leq 0.75$ , and non-dimensional thickness  $0.15 \leq l/d \leq 1.0$ . A theoretical model for the transmission loss combines 1D planar wave theory with end corrections for hole interaction effects. The model is based on the acoustic wavelength being much larger than the hole size. The predicted transmission loss is in very good agreement with the experimental measurement, with errors of about 1.5 dB or less for  $d/l \leq 0.5$ . The present model provides much higher fidelity than theories of past works over most of the range of the experiments and is able to capture the resonance effect exhibited in thicker plates. A systematic analysis of the error between the present model and experiment does not show any specific trends versus plate thickness-to-diameter ratio or porosity.

## NOMENCLATURE

$A$	Area
$a$	Spacing between perforations
$c$	Speed of sound
$d$	Hole diameter
$D$	Characteristic length of lattice containing perforations
FFT	Fast Fourier transform
$f$	Frequency
$i$	$\sqrt{-1}$
$I$	Incident pressure amplitude
$K$	Bulk modulus
$k$	Acoustic wave number

$L_T$	Transmission loss
$l$	Plate thickness
$M$	Fok's function [Eq. (28)]
$Pr$	Prandtl number
$p'$	Acoustic pressure
$p_0$	Static pressure
$R_c$	Reflection coefficient
$R$	Reflected wave amplitude
$R_{m1m2}$	Cross correlation of microphones 1 and 2
SPL	Sound pressure level
$S$	Surface area
$T$	Transmitted pressure amplitude
$T_c$	Transmission coefficient
TMM	Transfer matrix method
$t$	Time
$u$	Particle velocity
$x$	Axial coordinate
$Z$	Acoustic impedance
$Z_0$	Characteristic impedance
$\alpha_\infty$	Geometric tortuosity
$\beta$	Perforation porosity
$\gamma$	Specific heat ratio
$\gamma^2$	Coherence
$\Delta L_T$	Difference in modeled and experimental transmission loss
$\varepsilon$	Perforation thickness correction
$\eta$	Stokes number
$\theta$	Inclination angle with respect to normal direction of plate surface
$\lambda$	Acoustic wavelength
$\mu$	Dynamic viscosity of air
$\xi$	Ratio of hole diameter to hole separation distance
$\Pi$	Acoustic power
$\rho$	Density of air
$\sigma$	Flow resistivity
$\tau$	time lag
$\psi$	Inverse of Fok's function
$\omega$	Angular frequency

## Subscripts

1	Region upstream of contraction
2	Region inside contraction
3	Region downstream of contraction
cav	Cavity
e	Effective
I	Incident
p	Perforation
t	Transmitted

<sup>1</sup>G. C. G. Hofmans, R. J. J. Boot, P. P. J. M. Durrieu, Y. Auregan, and A. Hirschberg, "Aeroacoustic response of a slit-shaped diaphragm in a pipe at low Helmholtz number. I. Quasi-steady results," *J. Sound Vib.* **244**(1), 35–56 (2001).

<sup>2</sup>V. Phong, S. Taghavi Nezhad, F. Liu, and D. Papamoschou, "Noise reduction of a turbofan bleed valve," AIAA Pap. 2012–0681 (2012).

<sup>3</sup>I. B. Crandall, *Theory of Vibration System and Sound* (Van Nostrand, New York, 1926), pp. 229.

<sup>4</sup>L. E. Kinsler, A. R., Frey, A. B. Coppens, and J. V. Sanders, *Fundamentals of Acoustics* (Wiley and Sons, New York, 1982), Chap. 12, 303 pp., Chap. 6, pp. 125.

- <sup>5</sup>Lord Rayleigh III, *The Theory of Sound* (Macmillan, Dover Publications, New York, 1945), Vol. II, Chap. 14, pp. 162–169.
- <sup>6</sup>V. A. Fok, “Teoreticheskoe issledovanie provodimosti kruglogo otverstiya v perogorodke, postavlennoi poperek trubyy (Theoretical study of the conductance of a circular hole, in a partition across a tube),” *Dokl. Akad. Nauk SSSR* **31**(9), 875–878 (1941).
- <sup>7</sup>V. S. Nesterov, “An experimental study of the acoustical conductivity of a circular orifice in a partition placed across a tube,” *Dokl. Akad. Nauk SSSR* **31**(9), 879–882 (1941).
- <sup>8</sup>U. Ingard, “On the theory and design of acoustic resonators,” *J. Acoust. Soc. Am.* **26**(6), 1037–1061 (1953).
- <sup>9</sup>J. Christensen, L. Martin-Moreno, and F. J. Garcia-Vidal, “Theory of resonant acoustic transmission through subwavelength apertures,” *Phys. Rev. Lett.* **101**(1), 1–4 (2008).
- <sup>10</sup>B. Hou, J. Mei, M. Ke, W. Wen, Z. Liu, J. Shi, and P. Sheng, “Tuning Fabry–Perot resonances via diffraction evanescent waves,” *Phys. Rev. B* **76**(5), 1–6 (2007).
- <sup>11</sup>B. Hou, J. Mei, M. Ke, Z. Liu, J. Shi, and W. Wen, “Experimental determination for resonance-induced transmission of acoustic waves through subwavelength hole arrays,” *J. Appl. Phys.* **104**(1), 1–5 (2008).
- <sup>12</sup>L. J. Sivian, “Acoustic impedance of small orifices,” *J. Acoust. Soc. Am.* **7**(2), 94–101 (1935).
- <sup>13</sup>U. Ingard and S. Labate, “Acoustic circulation effects and the nonlinear impedance of orifices,” *J. Acoust. Soc. Am.* **22**(2), 211–218 (1950).
- <sup>14</sup>U. Ingard and H. Ising, “Acoustic nonlinearity of an orifice,” *J. Acoust. Soc. Am.* **42**(1), 6–17 (1967).
- <sup>15</sup>H. Aygun and K. Attenborough, “The insertion loss of perforated porous plates in a duct without and with mean air flow,” *Appl. Acoust.* **69**(6), 506–513 (2008).
- <sup>16</sup>S. H. Lee, J. G. Ih, and K. S. Peat, “A model of acoustic impedance of perforated plates with bias flow considering the interaction effect,” *J. Sound. Vib.* **303**, 741–752 (2007).
- <sup>17</sup>J. F. Betts, “Experiments and impedance modeling of liners including the effect of bias flow,” Ph. D. dissertation, Virginia Polytechnic Institute, Blacksburg, VA, 2000.
- <sup>18</sup>K. T. Chen, “Study on the acoustic transmission loss of a rigid perforated screen,” *Appl. Acoust.* **47**(4), 303–318 (1996).
- <sup>19</sup>R. B. Tayong, T. Dupont, and P. Leclaire, “Experimental investigation of holes interaction effect on the sound absorption coefficient of micro-perforated panes under high and medium sound levels,” *Appl. Acoust.* **72**(10), 777–784 (2011).
- <sup>20</sup>T. H. Melling, “The acoustic impedance of perforates at medium and high sound pressure levels,” *J. Sound. Vib.* **29**(1), 1–65 (1973).
- <sup>21</sup>N. Atalla and F. Sgard, “Modeling of perforated plates and screens using rigid frame porous models,” *J. Sound. Vib.* **303**, 195–208 (2007).
- <sup>22</sup>Y. Champoux and J. F. Allard, “Dynamic tortuosity and bulk modulus in air-saturated porous media,” *J. Appl. Phys.* **70**(4), 1975–1979 (1991).
- <sup>23</sup>J. F. Allard, *Propagation of Sound in Porous Media: Modeling Sound Absorbing Materials* (Elsevier, New York, 2009), Chap. 5, pp. 90.
- <sup>24</sup>L. Jaouen and F.-X. Bécot, “Acoustical characterization of perforated facings,” *J. Acoust. Soc. Am.* **129**(3), 1400–1406 (2011).
- <sup>25</sup>M. L. Munjal, *Acoustics of Ducts and Mufflers With Application to Exhaust and Ventilation System Design* (Wiley and Sons, New York, 1987), Chap. 1, pp. 9–12.
- <sup>26</sup>J. E. Ffowcs Williams and A. P. Dowling, *Sound and Sources of Sound* (Halsted, New York, 1983), Chap. 3, pp. 65–67.
- <sup>27</sup>C. H. Gerhold and L. R. Clark, “Database of inlet and exhaust noise shielding for wedge-shaped airframe,” NASA/TM-2001-210840, NASA (2001).
- <sup>28</sup>A. Savitzky and M. J. E. Golay, “Smoothing and differentiation of data by simplified least squares procedures,” *Anal. Chem.* **36**, 1627–1639 (1964).
- <sup>29</sup>P. M. Morse and U. K. Ingard, *Theoretical Acoustics* (McGraw-Hill, New York, 1968), Chap. 9, pp. 509–513.
- <sup>30</sup>E. J. Rice, M. F. Heidmann, and T. G. Sofrin, “Modal propagation angles in a cylindrical duct with flow and their relation to sound absorption,” NASA/TM-79030, NASA (1979).
- <sup>31</sup>H. Estrada, P. Candelas, A. Uris, F. Belmar, F. Javier García de Abajo, and F. Meseguer, “Influence of lattice symmetry on ultrasound transmission through plates with subwavelength aperture arrays,” *Appl. Phys. Lett.* **95**(5), 051906 (2009).